

**Parameter Estimation for Fault
Diagnosis of an Automotive Engine
using Extended Kalman Filters**

Martin Gunnarsson

Reg nr: LiTH-ISY-EX-3160

5th November 2001

Parameter Estimation for Fault Diagnosis of an Automotive Engine using Extended Kalman Filters

Master's thesis

performed in **Vehicular Systems**,
Dept. of Electrical Engineering
at **Linköpings Universitet**

Performed for **DaimlerChrysler AG**


by **Martin Gunnarsson**

Reg nr: LiTH-ISY-EX-3160

Supervisor: **Thomas Stutte**
DaimlerChrysler AG
Mattias Nyberg
Linköpings Universitet

Examiner: **Lars Nielsen**
Linköpings Universitet

Linköping, 5th November 2001.

	Avdelning, Institution Division, Department Vehicular Systems, Dept. of Electrical Engineering		Datum Date 5th November 2001
	Språk Language <input type="checkbox"/> Svenska/Swedish <input checked="" type="checkbox"/> Engelska/English <input type="checkbox"/> _____	Rapporttyp Report category <input type="checkbox"/> Licentiatavhandling <input checked="" type="checkbox"/> Examensarbete <input type="checkbox"/> C-uppsats <input type="checkbox"/> D-uppsats <input type="checkbox"/> Övrig rapport <input type="checkbox"/> _____	ISBN _____ ISRN _____ Serietitel och serienummer ISSN Title of series, numbering _____ LITH-ISY-3160
URL för elektronisk version http://www.fs.isy.liu.se			
Titel Parameterskattning för diagnos av en bilmotor med hjälp av extended kalmanfilter Title Parameter Estimation for Fault Diagnosis of an Automotive Engine using Extended Kalman Filters Författare Martin Gunnarsson Author			
Sammanfattning Abstract <p>A nonlinear state space model of the DaimlerChrysler diesel engine OM611 is used. Three different faults in the air path have been taken under consideration: inlet manifold pressure sensor fault, air mass-flow sensor fault and leakage in the inlet manifold. These faults are modeled and added to the nonlinear state space model. The faults are assumed to be constant during estimation. An extended Kalman filter is used as an observer of the system in order to estimate the different fault-parameters. Only one fault-parameter is monitored at a time. Simulations with high inlet manifold pressure has turned out to give good results, the estimated fault-parameters are close to the true values. For simulations with low pressure in the inlet manifold are the results less good, probably due to model errors. The extended Kalman filter has proved to perform well in this type of application, as an observer for a diagnosis system of an automotive engine.</p>			
Nyckelord Extended Kalman Filter; Automotive Diesel Engine; Nonlinear Model; Keywords Fault Diagnosis			

Abstract

A nonlinear state space model of the DaimlerChrysler diesel engine OM611 is used. Three different faults in the air path have been taken under consideration: inlet manifold pressure sensor fault, air mass-flow sensor fault and leakage in the inlet manifold. These faults are modeled and added to the nonlinear state space model. The faults are assumed to be constant during estimation. An extended Kalman filter is used as an observer of the system in order to estimate the different fault-parameters. Only one fault-parameter is monitored at a time. Simulations with high inlet manifold pressure has turned out to give good results, the estimated fault-parameters are close to the true values. For simulations with low pressure in the inlet manifold are the results less good, probably due to model errors. The extended Kalman filter has proved to perform well in this type of application, as an observer for a diagnosis system of an automotive engine.

Keywords: Extended Kalman Filter; Automotive Diesel Engine; Non-linear Model; Fault Diagnosis

Preface

The work done during this thesis and the concepts contained in the thesis are described in the following chapters.

Chapter 1 , Introduction: Background to this thesis is presented.

Chapter 2, Observer: Major differences between normal Kalman filters and extended Kalman filter is presented in this chapter.

Chapter 3 , Model: This chapter is based on conference paper [1] except Section 3.4.4. A nonlinear state space model of the diesel engine OM611 will be presented. Also the different fault models are explained here.

Chapter 4, Implementation: Some implementation problems are discussed here.

Chapter 5, Results: The results from simulations are presented in this chapter.

Chapter 6, Conclusion: Conclusions and future work is discussed in this chapter.

Acknowledgments

This work has been performed for DaimlerChrysler AG in both Linköping and Esslingen, Germany. I would like to thank my supervisors Mattias Nyberg, Lith, and Thomas Stutte, DaimlerChrysler, for their help and support. I would also like to thank all the people working at the engine team FT2/EA for making my stay in Germany pleasant and a time to remember. A special thanks goes to the people at Vehicular Systems for all the nice moments in the coffee room.

Martin Gunnarsson
Linköping, 5th November 2001

Contents

Abstract	v
Preface and Acknowledgment	vi
1 Introduction	1
1.1 Background	1
1.2 Objective	2
1.3 Limitations	2
2 Observer	3
2.1 Why an Observer?	3
2.2 Continuous Linear Kalman Filters	4
2.2.1 Property of the Linear Kalman Filter	5
2.3 Processes Described by Nonlinear Models	6
2.3.1 Linearization About a Point	7
2.4 Continuous Extended Kalman Filter	8
3 Model Development	11
3.1 Engine Description	11
3.2 Model Inputs and Output	12
3.3 Model of OM611 in the Fault-Free Case	12
3.3.1 Model Validation	14
3.4 Modeling of Faults	14
3.4.1 No Fault	14
3.4.2 Inlet Pressure Sensor Fault	15
3.4.3 Mass-Flow Sensor Fault: One Parameter Model	15
3.4.4 Mass-Flow Sensor Fault: Two Parameter Model	15
3.4.5 Manifold Leakage	19
4 Implementation	21
4.1 Complete State-Space Model of the Faulty Engine	21
4.2 Linearization Tool	22
4.3 Implementation of Kalman filters	23

5	Experimental results	25
5.1	Recapitulation of how a diagnosis system can work	25
5.2	Performances of the different filters	25
5.2.1	IPS-filter	26
5.2.2	HFM1-filter	27
5.2.3	HFM2-filter	29
5.2.4	ML-filter	30
5.2.5	Summary	33
5.3	When should the estimation be stopped?	33
5.3.1	Experimental results	34
5.3.2	Summary	34
6	Conclusions and Future Work	37
6.1	Conclusion	37
6.2	Future Work	38
	References	39
	Notation	41

Chapter 1

Introduction

This master thesis has been performed for DaimlerChrysler AG, Research and Technology (FT2/EA). DaimlerChrysler is one of the worlds biggest automotive producers and is responsible for brands like: Mercedes Benz, Chrysler, Smart, and Freightliner.

1.1 Background

The last decades more and more rigorous demands regarding emissions from automotive engines has led to more refined methods to achieve these requirements. When new hardware is installed to fulfill these requirements then there also has to be a way to decide whether this hardware is working as it should or if it is faulty. This is done by an on board diagnosis system (OBD-system) and its importance has increased over the last years. Since year 2000, see [1], all cars sold within EU must be equipped with a OBD-system.

One way of building a diagnosis system is to make a model of the process that we want to supervise. By letting an observer estimate some parameters and compare these estimated parameter values with the respective measured value, can one perform a diagnosis of the system.

The objective of this thesis have been to design an observer for a diagnosis system. The system is described by a nonlinear state space model. One observer that have turned out to give good results in other situations is the Kalman filter. The Kalman filter is derived for linear system but there also exist a version of this filter for nonlinear cases, the extended Kalman filter.

One important part of the diagnosis requirements for automotive engines are the components in the air path. Possible faults includes sensor faults, actuator faults, and leakages. These types of faults typically lead to degraded emission control, and also possible damage to engine compo-

nents.

1.2 Objective

The goal of this thesis was to investigate whether extended Kalman filters (EKF) can be used for fault-parameter estimation in a diagnosis system of a automotive engine. The faults that has been taking under consideration are inlet pressure sensor fault, air mass-flow sensor fault and leakage in the inlet manifold.

1.3 Limitations

Faults in the sensors are typically slow varying and affects the measurements as offset or scale factors. Also leakages are assumed slow varying. During simulation are all faults assumed to be constant. It is also assumed that only one fault at a time is present.

Chapter 2

Observer

This chapter will present one idea of how to use an observer in a diagnosis system. One example of an observer that can be used is the Kalman filter. Since the process in this thesis only can be satisfactory described by a nonlinear model, the extended version of the Kalman filter is used. The major differences between the normal Kalman filter and the extended Kalman filter will also be discussed in this chapter.

2.1 Why an Observer?

Why do we need an observer? The answer to this question is that we can not always measure all parameters of interest in a process. We can then make a model of the process and try to estimate the parameters of interest.

Assume there exist a model of the process of interest and that all signals into the process, $u(t)$, and all signals out from it, e.g. measured output $y(t)$, are recorded. Lets say that one parameter in this model describes a possible fault in the process. It is then of interest to determine if this model can describe the behavior of the process.

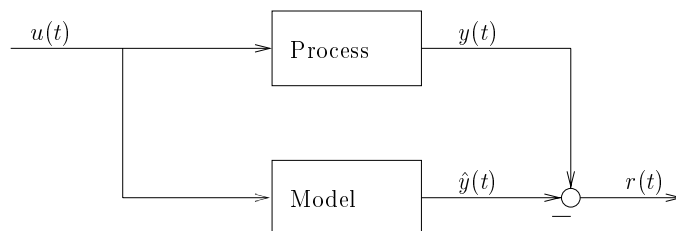


Figure 2.1: Simple fault detection system.

If we run the model with the same inputs as to the true process we will get an estimate of this fault-parameter. The fault-parameter is then fixed to this estimated value and the observer is run once more with the same inputs. This presumes that the fault is constant during estimation. If the fault-parameter can describe the actual fault in the process, the difference, $r(t)$ also called the residual, between the measured output from the process, $y(t)$, and the estimated output from the model, $\hat{y}(t)$, will be small, ideally zero. The principal is shown in Figure 2.1. If, on the other hand, the model with the fixed estimated fault-parameter can not describe the behavior of the process, the difference between the measured and estimated output will be large.

This is one way of designing a model-based diagnosis-system for an automotive engine. A more thorough introduction to model based diagnosis is given in [2].

There exist different types of observers but in this thesis the focus will be on the Kalman filters which will be described in the following sections. There exist two version of the Kalman filter, the normal one derived for linear systems and an extended version for nonlinear systems. Since the process, an automotive engine, best is described by a nonlinear model, the extended Kalman filter is used. The model of the process will be presented in Chapter 3.

2.2 Continuous Linear Kalman Filters

Usually is the discrete Kalman filter used in for industrial applications but in this thesis will the continuous Kalman filter be used instead. This is due to the existing model of the actual process, see Chapter 3, is continuous. One other reason is that *Matlab/Simulink* provides support for continuous models for simulations.

The continuous linear time-variant Kalman filter is derived for processes that can be described by linear state space models, according to conditions in Table 2.1. It is assumed that $v(t)$ and $w(t)$ are white noise processes uncorrelated with $x(0)$ and with each other.

	Model
Plant	$\dot{x}(t) = A(t)x(t) + B(t)u(t) + G(t)w(t)$
Measurement	$y(t) = C(t)x(t) + v(t)$
Plant noise	$w(t) \sim \mathcal{N}(0, Q(t))$
Measurement noise	$v(t) \sim \mathcal{N}(0, R(t))$

Table 2.1: Linear plant and measurement models.

If the process can be described by a linear model, a Kalman filter can be used as an observer of this process. Table 2.2 contains the equations describing the continuous linear Kalman filter.

	Continuous Kalman filter
Assumption	$x(0) \sim \mathcal{N}(x_0, P_0)$
Estimate update	$\dot{\hat{x}}(t) = A(t)\hat{x}(t) + B(t)u(t) + K(t)[y(t) - C(t)\hat{x}(t)]$
Covariance update	$\dot{P}(t) = A(t)P(t) + P(t)A^T(t) + G(t)Q(t)G^T(t) - K(t)R(t)K^T(t)$
Kalman gain	$K(t) = P(t)C^T(t)R^{-1}(t)$

Table 2.2: Continuous linear Kalman filter equations.

The initial value $x(0)$ is supposed to be a Gaussian process with known mean x_0 and covariance matrix P_0 .

2.2.1 Property of the Linear Kalman Filter

A time-invariant system is assumed here. The estimation error is

$$\tilde{x}(t) = x(t) - \hat{x}(t)$$

If substituting plant and measurement model into estimate update equation for the Kalman filter from Table 2.2 we get the following equation

$$\dot{\tilde{x}} = [A - K(t)C]\tilde{x} + Gw - Kv \quad (2.1)$$

This equation is driven by the measurement and process noise. If $[A - K(t)C]$ tend to an asymptotically stable matrix as $t \rightarrow \infty$, then in the limit the estimate $\hat{x}(t)$ converges to the expected true plant state $x(t)$.

A system is *detectable* if $A - KC$ can be made asymptotically stable by some matrix K . This implies that all unstable modes in A must be observable.

If a system is detectable then we know that $\hat{x}(t)$ will converge towards the expected true plant state $x(t)$.

The solution to the error update equation

$$\dot{P} = AP + PA^T + GQG^T - KRK^T \quad (2.2)$$

tends to a bounded steady-state value P if

$$\lim_{t \rightarrow \infty} P(t) = P$$

is bounded. In this case, for large t , $\dot{P}(t) = 0$ so that (2.2) tends to the algebraic Riccati equation

$$0 = AP + PA^T + GQG^T - KRK^T$$

If we in beforehand know that a system is detectable then the following theorem provides us with some useful information.

Theorem 2.1 *Let Q be a symmetric positive semidefinite matrix and R is a positive definite matrix. Suppose that $(A, G\sqrt{Q})$ is controllable. Then is (A, C) detectable if and only if:*

- *There is a unique positive definite solution P to (2.2) which is independent of $P(0)$. Furthermore, P is the unique positive definite solution to the algebraic Riccati equation.*
- *The steady-state error system defined by (2.1) with the steady-state Kalman gain*

$$K = PC^T R^{-1}$$

is asymptotically stable.

Since the system is detectable the theorem says that there exist a matrix P which is a solution to the algebraic Riccati equation and that there also exist a asymptotic stable Kalman gain K . Thence follows that the estimated state $\hat{x}(t)$ will converge toward the true state $x(t)$.

The proof of theorem 2.1 is found in [3]. For a more thorough description of the Kalman filter look in [4, 3].

2.3 Processes Described by Nonlinear Models

For some processes, a linear model is not a good description of the process. Suppose then, that the process can be described by the following nonlinear plant and measurement models, see Table 2.3. It is assumed that $v(t)$ and $w(t)$ are white noise processes uncorrelated with $x(0)$ and with each other.

	Model
Plant	$\dot{x}(t) = f(x(t), u(t), t) + G(t)w(t)$
Measurement	$y(t) = h(x(t), u(t), t) + v(t)$
Plant noise	$w(t) \sim \mathcal{N}(0, Q(t))$
Measurement noise	$v(t) \sim \mathcal{N}(0, R(t))$

Table 2.3: Nonlinear plant and measurement models

The functions f and h are continuously differentiable functions with respect of the state vector. The initial value $x(0)$ is supposed to be Gaussian process with known mean x_0 and covariance matrix P_0 , see [4].

As can be seen in Table 2.2, the error covariance update contains the state matrix $A(t)$ and the Kalman gain equation contains the measurement matrix $C(t)$. Since the nonlinear model of the process doesn't contain these matrices, the continuous linear Kalman filter theory can not be used and a another approach is needed.

2.3.1 Linearization About a Point

One way of handling nonlinear systems is to do a first order Taylor approximation around a certain point \hat{x} . If the perturbation of the system is sufficiently small relative to the higher order terms in the in the Taylor expansion, these higher order terms can then be ignored beyond some order.

Let the symbol Δ denote perturbation from \hat{x} and

$$\begin{aligned}\Delta x(t) &= x(t) - \hat{x}(t) \\ \Delta y(t) &= y(t) - h(\hat{x}(t), u(t), t)\end{aligned}$$

Then

$$\begin{aligned}\Delta \dot{x}(t) &= f(x(t), u(t), t) - f(\hat{x}(t), u(t), t) \\ \dot{x}(t) &= f(x(t), u(t), t) \\ &= f(\hat{x}(t), u(t), t) + \left. \frac{\partial f(x(t), u(t), t)}{\partial x(t)} \right|_{x=\hat{x}(t)} \Delta x(t)\end{aligned}$$

or

$$\begin{aligned}\Delta \dot{x}(t) &= f(x(t), u(t), t) - f(\hat{x}(t), u(t), t) \\ &= \left. \frac{\partial f(x(t), u(t), t)}{\partial x(t)} \right|_{x=\hat{x}(t)} \Delta x(t) + \text{higher-order terms}\end{aligned}$$

If the higher order terms can be neglected, then

$$\Delta \dot{x}(t) = F(t) \Delta x(t)$$

and the first-order approximation coefficient are given by

$$\begin{aligned}F(t) &= \left. \frac{\partial f(x(t), u(t), t)}{\partial x(t)} \right|_{x=\hat{x}(t)} \\ &= \left[\begin{array}{cccc} \frac{\partial f_1}{\partial x_1} & \frac{\partial f_1}{\partial x_2} & \cdots & \frac{\partial f_1}{\partial x_n} \\ \frac{\partial f_2}{\partial x_1} & \frac{\partial f_2}{\partial x_2} & \cdots & \frac{\partial f_2}{\partial x_n} \\ \vdots & \vdots & \ddots & \vdots \\ \frac{\partial f_n}{\partial x_1} & \frac{\partial f_n}{\partial x_2} & \cdots & \frac{\partial f_n}{\partial x_n} \end{array} \right] \Bigg|_{x=\hat{x}(t)}\end{aligned}$$

That is $F(t)$ is an $n \times n$ matrix.

The same idea is used for the measurement equation h , which will lead to

$$\begin{aligned}y(t) &= h(x(t), u(t), t) = h(\hat{x}(t), u(t), t) + \left. \frac{\partial h(x(t), u(t), t)}{\partial x(t)} \right|_{x=\hat{x}(t)} \Delta x(t) \\ &+ \text{higher-order terms}\end{aligned}$$

or

$$\Delta y(t) = \left. \frac{h(x(t), u(t), t)}{\partial x(t)} \right|_{x=\hat{x}(t)} \Delta x(t) + \text{higher-order terms}$$

If the higher-order terms in the Taylor expansion can be neglected the perturbation can be represented as

$$\Delta y(t) = H(t)\Delta x(t)$$

where the first-order approximation coefficient are given by

$$H(t) = \left. \frac{\partial h(x(t), u(t), t)}{\partial x(t)} \right|_{x=\hat{x}(t)}$$

$$= \begin{bmatrix} \frac{\partial h_1}{\partial x_1} & \frac{\partial h_1}{\partial x_2} & \cdots & \frac{\partial h_1}{\partial x_n} \\ \frac{\partial h_2}{\partial x_1} & \frac{\partial h_2}{\partial x_2} & \cdots & \frac{\partial h_2}{\partial x_n} \\ \vdots & \vdots & \ddots & \vdots \\ \frac{\partial h_l}{\partial x_1} & \frac{\partial h_l}{\partial x_2} & \cdots & \frac{\partial h_l}{\partial x_n} \end{bmatrix} \bigg|_{x=\hat{x}(t)}$$

This means that $H(t)$ is an $l \times n$ matrix.

The matrixes $A(t)$ and $C(t)$ in the equations for the linear continuous Kalman filter will be replaced with $F(t)$ and $H(t)$ respectively to handle the nonlinear process model.

2.4 Continuous Extended Kalman Filter

The major difference between the normal Kalman filter and the extended Kalman filter is how we handle the error covariance update and Kalman gain. In the extended Kalman filter we have to do a Taylor expansion of the process model and use these approximations in the Kalman gain and error covariance update.

The necessary conditions and the continuous extended Kalman filter equations are summarized in Table 2.4 and 2.5.

	Model
Plant	$\dot{x}(t) = f(x(t), u(t), t) + G(t)w(t)$
Measurement	$y(t) = h(x(t), u(t), t) + v(t)$
Assumption	$w(t)$ and $v(t)$ are white noise processes uncorrelated with $x(0)$ and each other
Plant noise	$w(t) \sim \mathcal{N}(0, Q(t))$
Measurement noise	$v(t) \sim \mathcal{N}(0, R(t))$

Table 2.4: Nonlinear plant and measurement models

	Continuous extended Kalman filter
Assumption	$x(0) \sim \mathcal{N}(x_0, P_0)$
Estimate update	$\dot{\hat{x}}(t) = f(\hat{x}(t), u(t), t) + K(t)[y(t) - h(\hat{x}(t), u(t), t)]$
Linear approximation	$F(t) \approx \left. \frac{\partial f(x(t), u(t), t)}{\partial x} \right _{x=\hat{x}(t)}$ $H(t) \approx \left. \frac{\partial h(x(t), u(t), t)}{\partial x} \right _{x=\hat{x}(t)}$
Covariance update	$\dot{P}(t) = F(t)P(t) + P(t)F^T(t) + G(t)Q(t)G^T(t) - K(t)R(t)K^T(t)$
Kalman gain	$K(t) = P(t)H^T(t)R^{-1}(t)$

Table 2.5: Continuous extended Kalman filter equations.

The reason of using an extended Kalman filter comes from the fact that normal Kalman filters has turned out to be powerful in effect and simple in form. The extended filter is then a natural extension of the linear methods for nonlinear systems.

One of the drawbacks of the extended Kalman filter is that it is computational heavy. The linearization must be evaluated in every point. The corresponding theory to the Theorem 2.1 does not exist for the nonlinear case, which is also is a big drawback. It then unfortunately become a problem of type, try and see if it works.

Chapter 3

Model Development

This chapter is based on conference paper [1], except Section 3.4.4.

3.1 Engine Description

The process in this thesis is a diesel engine, the Mercedes-Benz OM611, with 2.2 liter displacement and direct ignition. Detailed information about the engine can be found in [5]. A principle illustration is shown in Figure 3.1. The air entering the engine is measured by an air-mass flow-meter (HFM). It then passes the compressor and the CAC (Charge Air Cooler), enters the intake manifold, and flows into the cylinders. On the exhaust side, a part of the exhausts drives the turbine, and a part is recycled via the EGR (Exhaust Gas Recycling) path.

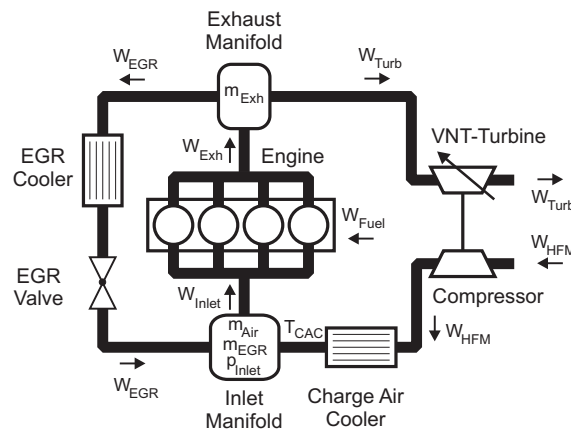


Figure 3.1: The Mercedes-Benz OM611 diesel engine.

3.2 Model Inputs and Output

The model of the engine is created to capture the performance in the air path. The characteristics of CAC and Compressor is not included in the model.

The production version of this engine is equipped with sensors measuring in-flowing air W_{HFM} , the temperature after charge air cooler (CAC) T_{Inter} and inlet manifold pressure p_{Inlet} . The inputs to the engine are W_{Fuel} , the turbine vane position X_{VNT} , and the effective EGR-valve area A_{EGR} .

The model of the engine uses the same actuator and sensor signals as the real engine, plus an additional input, normalized mass-flow of fuel, $W_{Fuelmap}$. The inputs to the model can be seen in Table 3.1.

inputs	explanation
A_{EGR}	effective area of EGR valve
N_{Eng}	engine speed
P_{Atm}	atmospheric pressure
T_{Inter}	temperature after CAC
W_{Fuel}	mass-flow of fuel
$W_{Fuelmap}$	normalized mass-flow of fuel
W_{HFM}	air mass-flow past the air mass-flow sensor
X_{VNT}	position of VNT vanes

Table 3.1: Signals used as inputs to the engine model

Output from the model is the inlet manifold pressure, p_{Inlet} . This value is then compared with the true inlet manifold pressure from the engine.

3.3 Model of OM611 in the Fault-Free Case

The model used for the Kalman filter design is based on principles described in [6, 7, 8, 9].

Engine Model in the Fault-Free Case

The model of the OM611 engine for the fault free case is as follows:

$$\dot{p}_{Inlet} = \frac{1}{V_{Inlet}} \left(\frac{R_{Air} c_{p,Air}}{c_{v,Air}} W_{HFM} T_{Inter} + \frac{R_{Exh} c_{p,Exh}}{c_{v,Exh}} W_{EGR} T_{EGR} - \frac{R_{Inlet} c_{p,Inlet}}{c_{v,Inlet}} W_{Inlet} T_{Inlet} \right) \quad (3.1)$$

$$\dot{m}_{Air} = W_{HFM} - \frac{m_{Air}}{m_{Air} + m_{EGR}} W_{Inlet} \quad (3.2)$$

$$\dot{m}_{EGR} = W_{EGR} - \frac{m_{EGR}}{m_{Air} + m_{EGR}} W_{Inlet} \quad (3.3)$$

$$\dot{m}_{Exh} = W_{Exh} - W_{Turb} - W_{EGR} \quad (3.4)$$

where

$$W_{EGR} = \frac{A_{EGR} p_{Exh}}{\sqrt{R_{Exh} T_{Exh}}} \Psi_{\kappa_{Exh}} \left(\frac{p_{Inlet}}{p_{Exh}} \right) \quad (3.5)$$

$$\Psi_{\kappa} \left(\frac{p_1}{p_0} \right) = \begin{cases} \sqrt{\frac{2\kappa}{\kappa-1} \left\{ \left(\frac{p_1}{p_0} \right)^{\frac{2}{\kappa}} - \left(\frac{p_1}{p_0} \right)^{\frac{\kappa+1}{\kappa}} \right\}} & \text{if } \left(\frac{p_1}{p_0} \right) \geq \left(\frac{2}{\kappa+1} \right)^{\frac{\kappa}{\kappa-1}} \\ \sqrt{\kappa \left(\frac{2}{\kappa+1} \right)^{\frac{\kappa+1}{\kappa-1}}} & \text{otherwise} \end{cases} \quad (3.6)$$

$$W_{Inlet} = f(N_{Eng}, \frac{p_{Inlet}}{T_{Inlet} R_{Inlet}}) \frac{N_{Eng} p_{Inlet}}{T_{Inlet} R_{Inlet}} \frac{V_{Eng}}{120} \quad (3.7)$$

$$W_{Exh} = W_{Inlet} + W_{Fuel} \quad (3.8)$$

$$W_{Turb} = \frac{p_{Exh}}{\sqrt{T_{Exh}}} g \left(\frac{p_{Exh}}{p_{Atm}}, X_{VNT} \right) \quad (3.9)$$

$$T_{Exh} = T_{Inlet} + \frac{Q_{LHV} h(W_{Fuelmap}, N_{Eng})}{c_{p,Exh} (W_{Inlet} + W_{Fuel})} \quad (3.10)$$

$$p_{Exh} = \frac{m_{Exh} R_{Exh} T_{Exh}}{V_{Exh}} \quad (3.11)$$

$$c_{p,Inlet} = c_{v,Inlet} + R_{Inlet} \quad (3.12)$$

$$c_{v,Inlet} = \frac{c_{v,Air} m_{Air} + c_{v,Exh} m_{EGR}}{m_{Air} + m_{EGR}} \quad (3.13)$$

$$R_{Inlet} = \frac{R_{Air} m_{Air} + R_{Exh} m_{EGR}}{m_{Air} + m_{EGR}} \quad (3.14)$$

$$T_{Inlet} = \frac{p_{Inlet} V_{Inlet}}{(m_{Air} + m_{EGR}) R_{Inlet}} \quad (3.15)$$

$$T_{EGR} = 831K \quad (3.16)$$

The model contains three static functions: f , h , and g . They are represented as interpolation in lookup tables (maps). Also the $\Psi_{\kappa}(\cdot)$ -function is implemented as interpolation in a lookup table. The parameters and lookup tables in the model were obtained partly from manufacturer data, and partly from steady state and dynamic measurements.

The presented model is assumed to be valid in the fault-free case. When there is a fault present, other models are valid and these will be described later in Section 3.4.

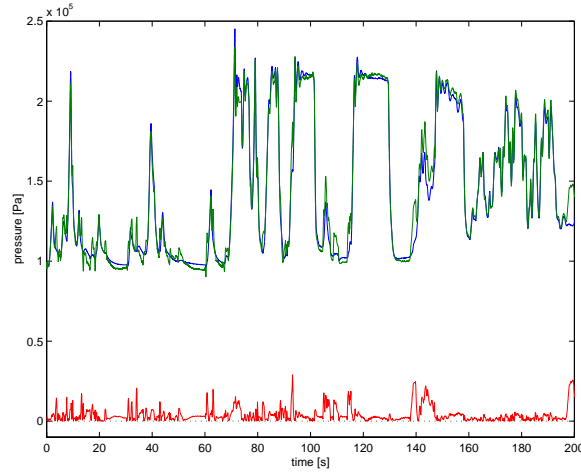


Figure 3.2: Simulated and measured inlet pressure p_{Inlet} (upper lines). The absolute value of the difference (lower line).

3.3.1 Model Validation

The model described above is simulated and a comparison with real measurement data can be seen in Figure 3.2. The figure shows the simulated and measured inlet pressure p_{Inlet} . The agreement is quite good but some model errors can be seen for highly dynamic parts. Also longer measurements were compared and on average, an RMS error of 3% was obtained.

3.4 Modeling of Faults

There are three different fault types taken into consideration, inlet pressure sensor fault (IPS), air mass-flow sensor fault modeled in two different ways ($HFM1$ & $HFM2$) and manifold leakage (ML).

3.4.1 No Fault (NF)

The model for the fault free engine was described in Section 3.3. To completely describe the NF fault-mode, we also add equations describing that the sensors and actuators are fault free.

$$W_{HFM,s} = W_{HFM} \quad (3.17a)$$

$$T_{Inlet,s} = T_{Inlet} \quad (3.17b)$$

$$p_{Inlet,s} = p_{Inlet} \quad (3.17c)$$

$$N_{Eng,s} = N_{Eng} \quad (3.17d)$$

$$p_{Atm,s} = p_{Atm} \quad (3.17e)$$

$$A_{EGR} = A_{EGR,r} \quad (3.17f)$$

$$W_{Fuel} = W_{Fuel,r} \quad (3.17g)$$

$$X_{VNT} = X_{VNT,r} \quad (3.17h)$$

Here, index s indicates sensor value and index r indicates reference value, set by the controller. For example, equation (3.17a) says that the measured value $W_{HFM,s}$ is equal to the physical variable W_{HFM} .

3.4.2 Inlet Pressure Sensor Fault (*IPS*)

The model for the fault mode *IPS* is obtained by taking the model for the *NF* fault-mode but replacing equation (3.17c) with

$$p_{Inlet,s} = k p_{Inlet} \quad (3.18)$$

where k is an unknown constant, and $k \neq 1$.

3.4.3 Mass-Flow Sensor Fault: One Parameter Model (*HFM1*)

The mass-flow sensor fault is modeled in two ways. One model with one fault-parameter (*HFM1*) and one with two fault-parameters *HFM2*. In the first model the gain in the sensor is proportional towards the true mass-flow.

The model for fault mode *HFM1* is obtained by taking the model for the *NF* fault-mode but replacing equation (3.17a) with

$$W_{HFM,s} = g W_{HFM} \quad (3.19)$$

where g is an unknown constant, and $g \neq 1$.

3.4.4 Mass-Flow Sensor Fault: Two Parameter Model (*HFM2*)

A typical mass-flow sensor fault has been measured. Its characteristics can be seen in Figure 3.3. The sensor have a variable gain-fault and the gain is defined in percentage as

$$\frac{\text{measured mass-flow} - \text{true mass-flow}}{\text{true mass-flow}} \cdot 100 + 100$$

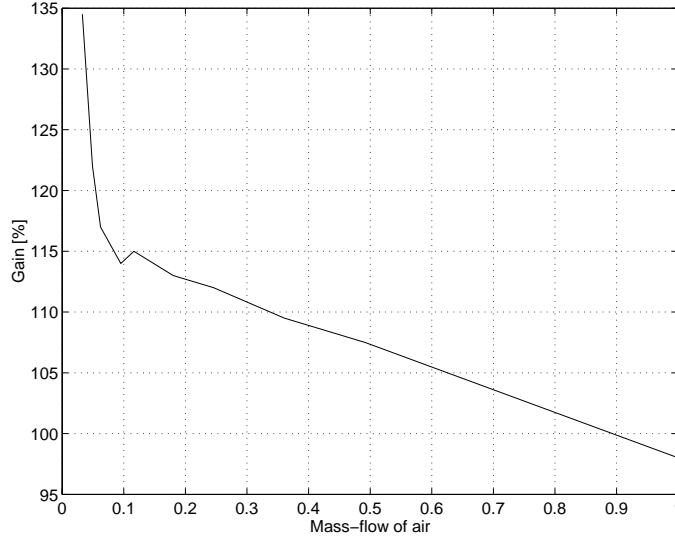


Figure 3.3: Measured gain-fault in a mass-flow sensor

For low mass-flows of air through the sensor the measured mass-flow is almost 35% higher than the true mass-flow. For high mass-flows the measured mass-flow is approximately 98% of the true mass-flow, that is 2% less than the actual mass-flow, and then more or less fault free. This sensor-fault can be modeled as follows:

$$W_{HFM,s} = f(W_{HFM})W_{HFM}$$

Where $f(\cdot)$ is a function describing the gain in the sensor and is seen as a function of the real mass-flow through the sensor. As described in Section 3.2 W_{HFM} is an input signal to the model and is therefore to be explicitly found.

We can then model the gain-fault as

$$W_{HFM} = g(W_{HFM,s})W_{HFM,s}$$

where the gain $g(W_{HFM,s})$ is defined as

$$\frac{1}{f(W_{HFM})}$$

The gain $g(\cdot)$ is looked upon as a function of the measured mass-flow through the sensor. The characteristics of the gain-fault as a function of the measured mass-flow can be seen in Figure 3.4. For low measured mass-flows the true mass-flow through the sensor is approximately 75% of

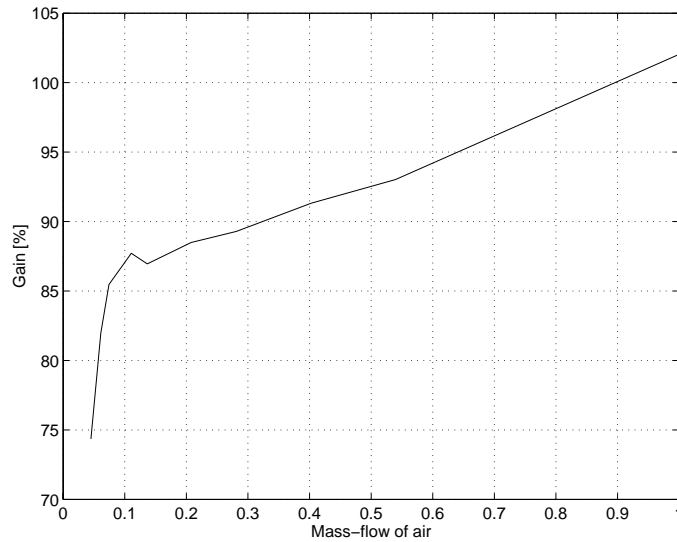


Figure 3.4: The gain in a mass-flow sensor as a function of the measured mass-flow.

the measured mass-flow. For high mass-flows the sensor is more or less fault free, as said before.

When the gain $g(\cdot)$ is plotted as a function of the logarithmic mass-flow, as in Figure 3.5, solid line, the gain can be approximated with a first order polynomial:

$$g(W_{HFM,s}) = a + b \log_{10} W_{HFM,s}$$

The polynomial coefficients that best approximate the gain for all mass-flows in Figure 3.5, in least-square sense, dashed line, is

$$a = 1.11 \quad b = 0.15.$$

For high respective low mass-flows these coefficients do not describe the gain-fault in a good way. For high mass-flows are

$$a_{high} = 1.19 \quad b_{high} = 0.23$$

a better approximation of the coefficients, see Figure 3.5 the dotted line. The polynomial coefficients that best approximate, in least-square sense, low mass-flows are

$$a_{low} = 1.48 \quad b_{low} = 0.34$$

See Figure 3.5 the dash-dotted line.

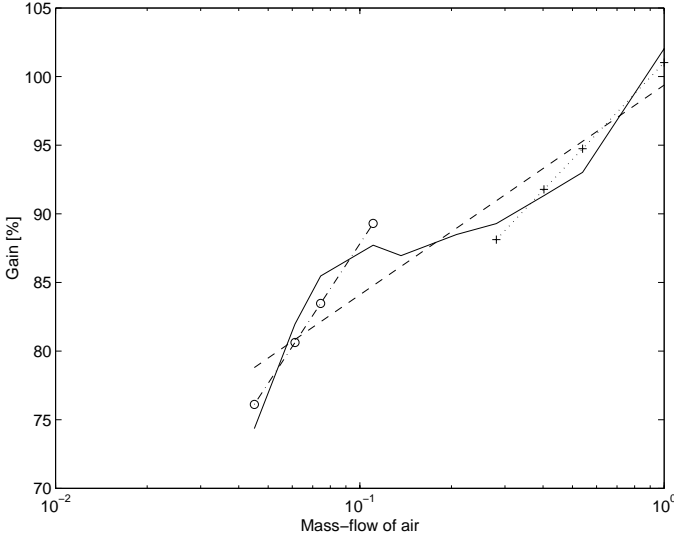


Figure 3.5: The gain $g(W_{HFM,s})$ plotted as a function of the logarithmic measured mass-flow, solid line, and a first order polynomial to approximate the gain, in least-square sense, dashed line. The dotted and dash-dotted lines are also first order polynomial to solely approximate high and low mass-flows respectively

Consequently, the model for fault mode *HFM2* is obtained by taking the model for the *NF* fault-mode but replacing equation (3.17a) with

$$W_{HFM} = (a + b \log_{10} W_{HFM,s}) W_{HFM,s} \quad (3.20)$$

where a, b are unknown constants, and $a \neq 1$ or $b \neq 0$.

The mass-flow sensor fault has been modeled in two ways. The first model, *HFM1*, will have problem to detect a fault in the sensor whose characteristics can be seen in Figure 3.3. For some mass-flows the gain fault is big but for other mass-flows the sensor is almost fault free. On the other hand the second model, *HFM2*, is more complicated and more computational power will be needed to simulate this model. Which model we choose is therefore a balance between how much computational power we have access to and how good we want the diagnosis system to be.

3.4.5 Manifold Leakage (*ML*)

It is assumed that the leakage occur in the inlet manifold and that the area of the hole is constant. The flow through the leakage is modeled as a flow through a restriction. This type of model has been validated in [8] with good results.

Equations (3.1), (3.2), and (3.3) in the fault-free model is replaced by

$$\begin{aligned} \dot{p}_{Inlet} &= \frac{1}{V_{Inlet}} \left(\frac{R_{Air} c_{p,Air}}{c_{v,Air}} W_{HFM} T_{Inlet} + \right. \\ &+ \frac{R_{Exh} c_{p,Exh}}{c_{v,Exh}} W_{EGR} T_{EGR} \\ &\left. - \frac{R_{Inlet} c_{p,Inlet}}{c_{v,Inlet}} (W_{Inlet} + W_{Leak}) T_{Inlet} \right) \quad (3.21) \end{aligned}$$

$$\dot{m}_{Air} = W_{HFM} - \frac{m_{Air}}{m_{Air} + m_{EGR}} (W_{Inlet} + W_{Leak}) \quad (3.22)$$

$$\dot{m}_{EGR} = W_{EGR} - \frac{m_{EGR}}{m_{Air} + m_{EGR}} (W_{Inlet} + W_{Leak}) \quad (3.23)$$

$$W_{Leak} = \frac{A_{Leak} p_{Inlet}}{\sqrt{R_{Inlet} T_{Inlet}}} \Psi_{\kappa_{Air}} \left(\frac{p_{Atm}}{p_{Inlet}} \right) \quad (3.24)$$

where

$$A_{Leak} \neq 0$$

and the function $\Psi_{\kappa}(\cdot)$ was defined in (3.6). All sensors and actuators are assumed fault free, and thus equations (3.17) are assumed to hold.

Chapter 4

Implementation

4.1 Complete State-Space Model of the Faulty Engine

The model of the engine in the fault free case is described by four state equations as was shown in Section 3.3.

For each fault mode, the model of the engine is obtained by adding and/or replacing equations according to Section 3.4. Since all fault-parameters are assumed constant the derivative of each fault parameter is zero.

As an example, a part of the five state equations that describes the IPS-fault model are:

$$\dot{x} = \begin{pmatrix} \dot{p}_{Inlet} \\ \dot{m}_{Air} \\ \dot{m}_{EGR} \\ \dot{m}_{Exh} \\ \dot{k} \end{pmatrix} = \begin{pmatrix} \frac{1}{V_{Inlet}} \left(\frac{R_{Air} c_{p,Air}}{c_{v,Air}} W_{HFM} T_{Inter} + \dots \right) \\ W_{HFM} - \frac{m_{Air}}{m_{Air} + m_{EGR}} W_{Inlet} \\ W_{EGR} - \frac{m_{EGR}}{m_{Air} + m_{EGR}} W_{Inlet} \\ W_{Exh} - W_{Turb} - W_{EGR} \\ 0 \end{pmatrix}$$

Of these five equations four describes the engine and the last one the fault parameter k . The model of the measurement equation

$$y = p_{Inlet}$$

is replaced by equation (3.18) and then becomes

$$y = k p_{Inlet}$$

Equation (3.5) to (3.16) are of course included to describe the the model of the *IPS*-fault completely.

The same methodology is used to create the remaining fault models. Each fault model is simulated in *Matlab/Simulink* and the results are presented in Section 5.2.

4.2 Linearization Tool

As been described in Chapter 2, and can be seen in Table 2.5, we need a linearization of the state-space model. The linearization is based on a first order Taylor approximation and therefore the partial derivatives of the fault models are calculated.

For the linearization of the different models a linearization tool was developed in *Mathematica*. The basic idea with this linearization tool is that the results from already calculated expressions and partial derivatives are reused, in order to save calculation time during simulation.

The principal of the linearization tool will be shown with the following example:

$$f(v, x, y, z) = vxz + vxz(1 + xy)$$

To evaluate $f(v, x, y, z)$ 2 additions and 6 multiplications will be needed. If we define $g(v, x, z)$ and $h(x, y)$, where

$$\begin{aligned} g(v, x, z) &= vxz \\ h(x, y) &= 1 + xy \end{aligned}$$

and

$$\bar{f}(g, h) = g(v, x, z) + g(v, x, z)h(x, y)$$

will this result in the exact same equation of $\bar{f}(g, h)$ as of $f(v, x, y, z)$:

$$\bar{f}(g, h) = g(v, x, z) + g(v, x, z)h(x, y) = vxz + vxz(1 + xy)$$

In this case will the evaluation of $\bar{f}(g, h)$ results in 2 additions and 4 multiplications. The latter way saves 2 multiplications.

If the partial derivative of $f(v, x, y, z)$ with respect to x is taken, one will get the following result:

$$\frac{\partial f(v, x, y, z)}{\partial x} = vz + vz(1 + xy) + vxzy$$

To compute the derivative there will be a need of 3 additions and 7 multiplications.

When we take the partial derivative of $\bar{f}(g, h)$ with respect to x we will obtain the following result:

$$\frac{\partial \bar{f}(g, h)}{\partial x} = \frac{\partial g(v, x, z)}{\partial x} + g(v, x, z) \frac{\partial h(x, y)}{\partial x} + \frac{\partial g(v, x, z)}{\partial x} h(x, y)$$

where

$$\begin{aligned} \frac{\partial g(v, x, z)}{\partial x} &= vz \\ \frac{\partial h(x, y)}{\partial x} &= y \end{aligned}$$

Since $g(v, x, z)$ and $h(x, y)$ are already evaluated, the evaluation of the partial derivative of $\hat{f}(g, h)$ with respect to x will result in 2 additions and 3 multiplications. Compared with the first way of calculating the partial derivative the latter way saves 4 multiplications and 1 addition due to the fact that already calculated expressions can be reused.

It is according to this principle the linearization tool works. The equations (3.5) to (3.15) are differentiated in the reversed order and saved as separate variables. Whenever an expression of an already calculated equation appears it is replaced by the corresponding variable. The linearized state-space model is saved as analytical expressions in a *m-file*. For every point that is simulated the *m-file* with the linearized state-space model is run.

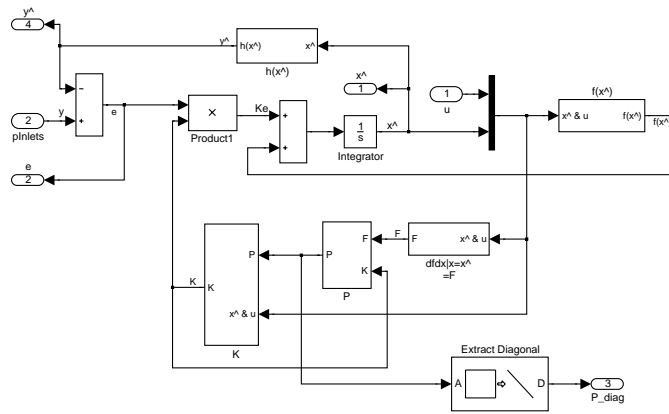


Figure 4.1: Simulink model of the extended Kalman filter.

4.3 Implementation of Kalman filters

The Kalman filters were implemented in *Matlab/Simulink*. The graphical environment of *Simulink* provides an easy way of implementing the equations in Table 2.5 that describes the extended Kalman filter. In Figure 4.1 can a part of this implementation be seen. One drawback of implementing the filters in *Simulink* is that it is computationally heavy and therefore takes long time.

The results from the linearization tool were saved as *m-files*. Also the different state-space models were saved as *m-files*. During simulation of a fault-model, the states are updated by running the *m-files* containing the state-space model and the linearized state-space model of the actual fault-model. This is handled by the block denoted $f(x^{\wedge}), h(x^{\wedge}), dfdx|x = x^{\wedge} = F$ and inside block K in Figure 4.1. The output from block $dfdx|x =$

$\hat{x} = F$ and block P are matrixes, all other signals are vectors. Block *Extract Diagonal* extracts the diagonal from the covariance matrix P . The diagonal of matrix P contains the variance of the different state variables.

Inputs to the *Simulink* model of the extended Kalman filter in Figure 4.1 are the measured pressure in the inlet manifold, denoted y , and the input signals from Table 3.1, denoted u . Output from the *Simulink* model are estimated inlet manifold pressure, denoted \hat{y} . Also the residual ($p_{Inlet} - \hat{p}_{Inlet}$), denoted e , the estimated state variables, denoted \hat{x} and the diagonal of the covariance matrix P , denoted P_diag are outputs from the *Simulink* model for help during tuning of the filters.

The extended Kalman filter based on the different fault models has turned out to be stiff. By rescaling the state p_{Inlet} from Pa to MPa the results during simulation has improved significantly. Also the fault-parameter A_{Leak} has been scaled, from m^2 to $m\ m^2$.

A lot of time have been spent on tuning the different Kalman filters in order to make them perform as desired. This is done by setting the elements in the covariance matrixes Q and R , see Table 2.4, to different values. By varying the element values one can e.g. decide how fast a fault-parameter shall converge. The faster the filter is the more sensible it is to disturbances. The final settings of the element values in matrixes Q and R are a compromise between how fast the filters should converge and how sensible it should be.

Chapter 5

Experimental results

In this chapter the results from the simulations are presented and discussed.

5.1 Recapitulation of how a diagnosis system can work

The idea with these different observers is that they should work in a diagnosis system. We simulate the different observers with the same data and determine the fault-parameters for each observer respectively. Then we run the observers once again with the same data and the fault-parameters fixed to the values determined in the previous simulation. By studying the residual, i.e. the difference between the measured inlet manifold pressure and the estimated inlet manifold pressure, a diagnosis can be determined. If the residual is small, then the actual fault-parameter can explain the behavior of the engine and we have a present fault. If on the other hand, the residual is large, then the actual fault-parameter can not explain the behavior of the engine and the that fault that this fault-parameter correspond to is rejected.

5.2 Performances of the different filters

The data for the simulations comes from driving sessions with a car equipped with the OM611 diesel engine on public roads. The faults in the sensors has been simulated. In the case of manifold leakage a hole with a known diameter has been made in the inlet manifold.

The figures in this section shows the estimated inlet manifold pressure, residual, estimated fault parameter, solid line, together with the true value of the fault-parameter, dashed line, and the covariance of the estimated

fault-parameter. In the figures of the *HFM*-faults the estimated inlet pressure plot is replaced with the plot of the measured mass-flow W_{HFM} .

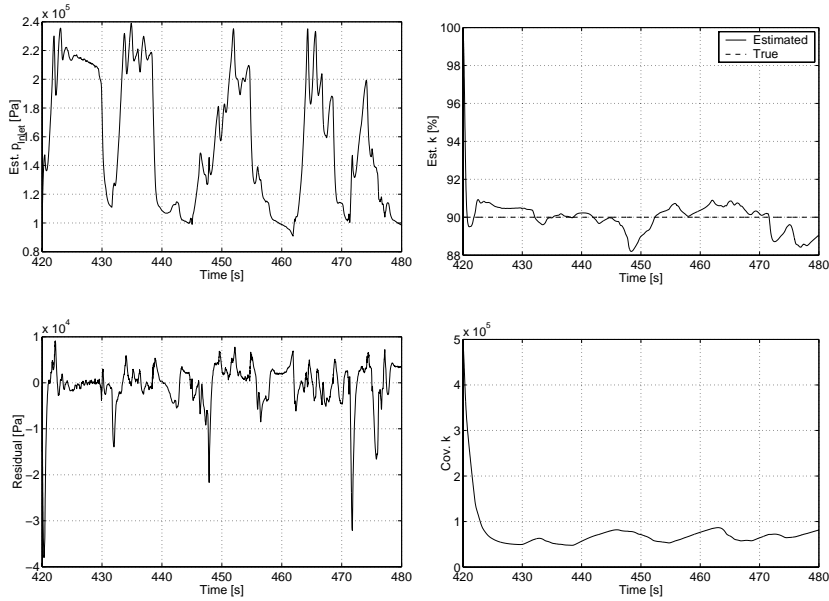


Figure 5.1: IPS-filter with high pressure in the inlet manifold and an IPS-fault present.

5.2.1 IPS-filter

The *IPS*-fault has been modeled as a static gain fault in the sensor. In this case a gain-fault of 0.9 has been used for validation of the IPS-filter, e.g. the sensor is measuring 90% of the true pressure. In Figure 5.1 can we see that the estimated gain converges fast and that it's varying only a few percentage around the true value.

A different behavior can be seen in Figure 5.2, the convergence is slow and it is only in the last few seconds of the simulation that we can say that it has converged toward a value. The lower the pressure in the inlet manifold is the slower the filter tends to converge in general. In this latter case there has been a low demand of torque from the driver resulting in a low inlet manifold pressure. At steady state the inlet manifold pressure is proportional to the output torque from the engine.

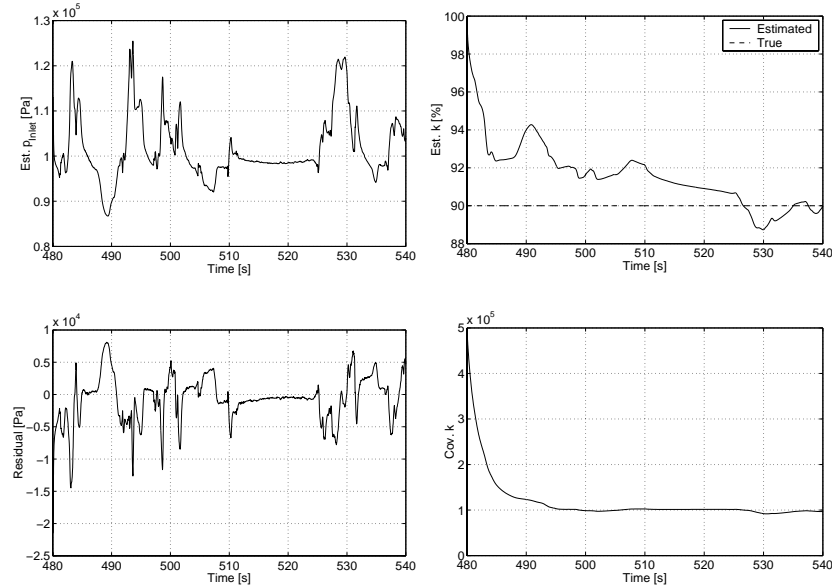


Figure 5.2: IPS-filter with low pressure in the inlet manifold and an IPS-fault present.

5.2.2 HFM1-filter

As with the *IPS*-fault the *HFM1*-fault is seen as a gain-fault. In this case the gain has been set to 1.1 during validation, e.g. the sensor measures a mass-flow through the CAC that is 10% higher than the actual mass-flow.

Figure 5.3 shows the behavior of the *HFM1*-filter when the mass-flow through the CAC is high. The filter converges fast with only a small variation of the estimate parameter \hat{g} .

In Figure 5.4 we can see the behavior of the *HFM1*-filter when the mass-flow through the CAC is low and with small variation. The filter converges quite fast but has unfortunately a negative bias of approximately 2%.

This is due to the low mass-flow and small variation in the input signals. One may think that an estimated parameter that is only two percent from the true value is good. But in this case, when the actual fault is simulated, the estimation should be better because the fault-model is “perfect”. One possible cause of this behavior is that the engine model has a bigger model error when the mass-flow is low compared to when the mass-flow through the CAC is high.

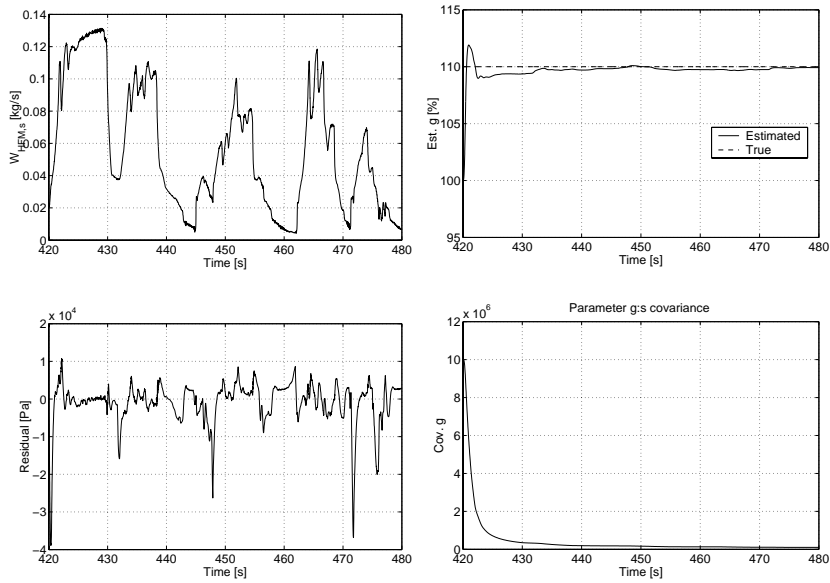


Figure 5.3: HFM1-filter with high mass-flow through the CAC and a HFM1-fault present.

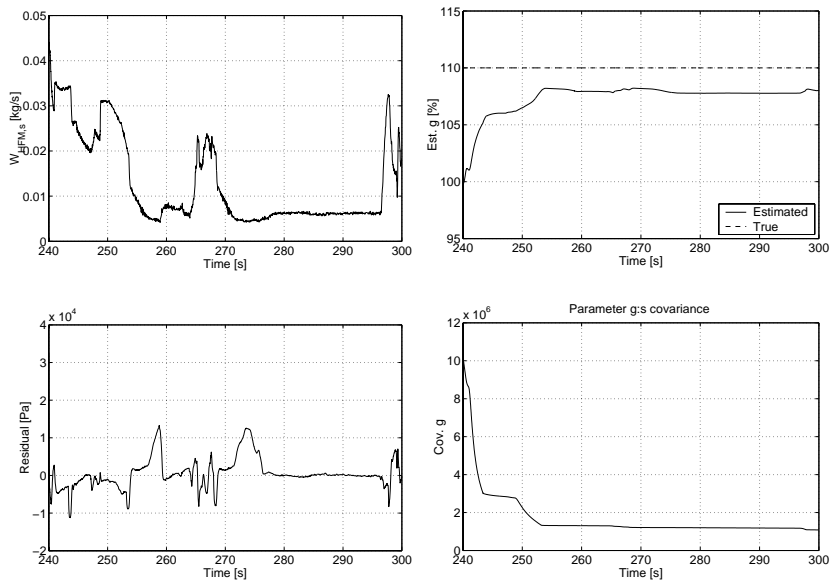


Figure 5.4: HFM1-filter with low mass-flow through the CAC and a HFM1-fault present.

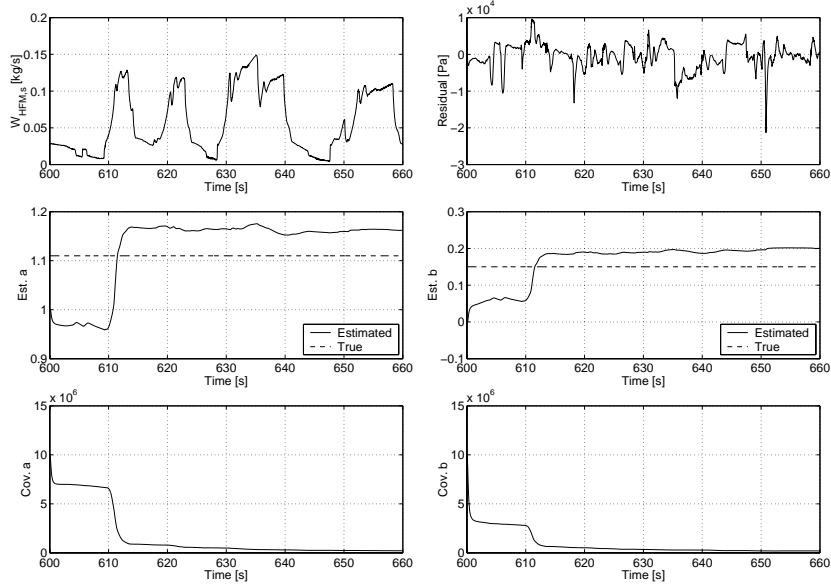


Figure 5.5: HFM2-filter with high mass-flow through the CAC and HFM2-fault present.

5.2.3 HFM2-filter

The *HFM2*-fault is based on a typical mass-flow sensor fault as described in Section 5.2.3. The coefficients that best explains the faulty mass-flow sensor for all mass-flows in Figure 3.5 were concluded to be $a = 1.11$ and $b = 0.15$. For high mass-flows were they concluded to be $a_{high} = 1.19$ and $b_{high} = 0.23$.

As can be seen in Figure 5.5 the estimated parameters \hat{a} and \hat{b} are in between these values. The estimated values are: $\hat{a} \approx 1.16$ and $\hat{b} \approx 0.2$. This seems reasonable, the mass-flow through the CAC is rather high and therefor should the estimated parameter values be closer to the coefficients that models the high mass-flow.

If the mass-flow through the CAC is low during simulation we will get a filter behavior as in Figure 5.6. In this case, the estimation of the both fault-parameters is really poor: $\hat{a} \approx 0.95$ and $\hat{b} \approx 0.05$. The parameter values that best explained low mass-flows where concluded to be $a_{low} = 1.48$ and $b_{low} = 0.34$ and the estimated fault-parameters are far from these values.

These values of the estimated fault-parameters suggest that the sensor is almost fault-free which it isn't. The actual fault is largest for low mass-flows. Why the estimated parameters values are far from the theoretical

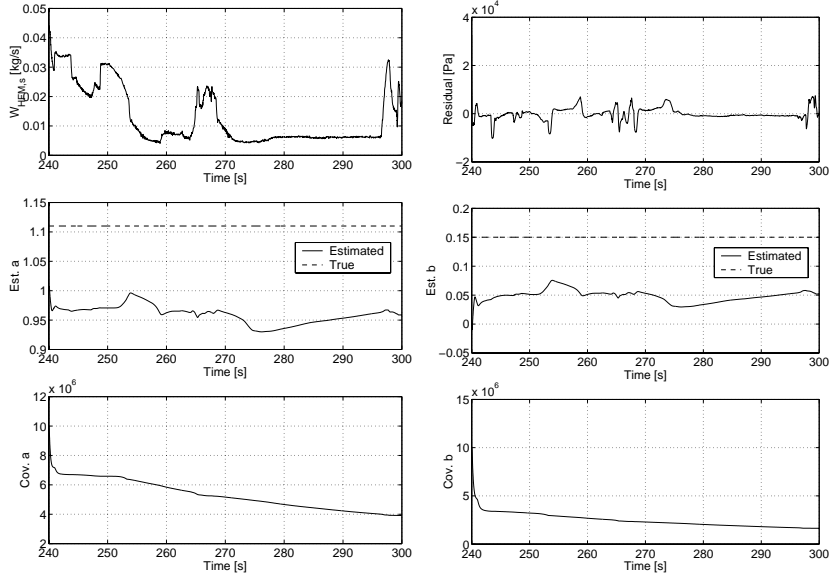


Figure 5.6: HFM2-filter with mass-flow through the CAC and HFM2-fault present.

values can be due to the fact that the over all model errors are larger when the mass-flows and thereby the inlet manifold pressure is low.

5.2.4 ML-filter

The *ML*-filter is modeled to estimate the leakage area between CAC and the cylinders. Figure 5.7 shows a simulation where a 4 mm hole has been made in the inlet manifold. In this case is the estimated leakage area $\hat{A}_{Leak} \approx 1.3 \cdot 10^{-5} \text{ m}^2$ which indicates a hole diameter of 4.1 mm . To be able to detect a hole there must a difference between the ambient pressure and the pressure in the inlet manifold. The bigger difference, the easier to detect.

In Figure 5.8 can we see an example when the difference between the ambient pressure and inlet manifold pressure is low. The estimated leakage area is far from the true value. Would it not have been for the last sudden increase in inlet pressure, would the estimated area \hat{A}_{Leak} be approximately $4 \cdot 10^{-7} \text{ m}^2$ which indicates a hole diameter of 0.7 mm . Far from the true value.

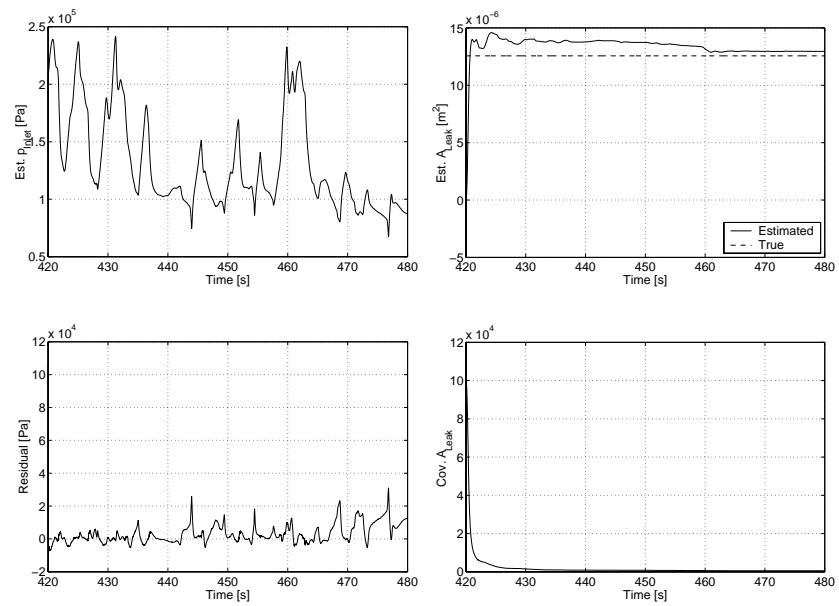


Figure 5.7: ML-filter with high pressure in the inlet manifold and 4 mm hole present.

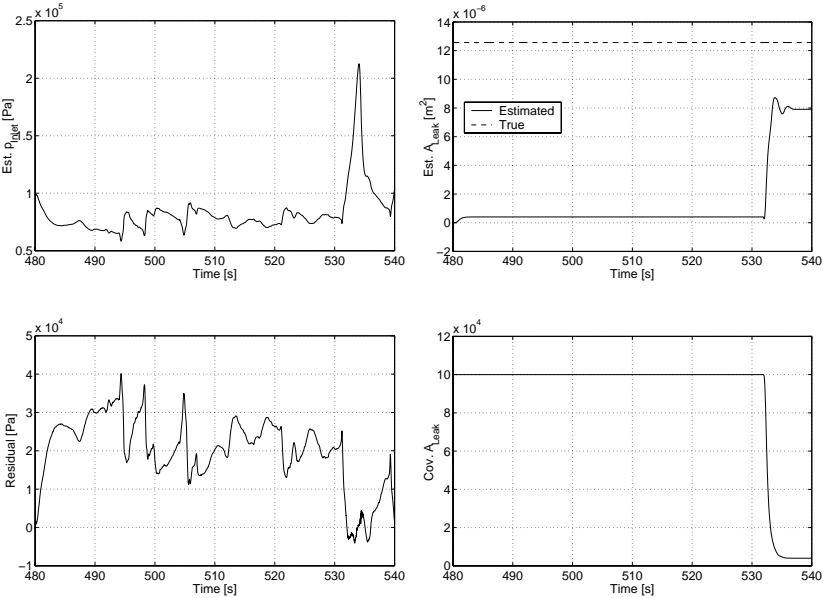


Figure 5.8: ML-filter with low pressure in the inlet manifold and 4 mm hole present.

5.2.5 Summary

For more or less all the filters, there is a demand for high pressure in the inlet manifold if the estimate is going to be good. When this is the case all filters worked well but when this is not the case, the estimates are poor. This problem makes it hard to rely on the filters; is the estimate good or is it a simulation where the variation in the input signals are low?

5.3 When should the estimation be stopped?

For a diagnosis system it is essential to be able to rely on the estimated parameter, otherwise will it be impossible to make the right decision. Bad estimated parameters can cause the diagnosis system to take decisions where the true fault is rejected.

The problem of estimating parameters is to know when the estimation is good enough. If the estimation is good enough there is no need for further estimation and computation time can be saved. If, on the other hand, the estimate is poor, more time for estimation is needed for a good result.

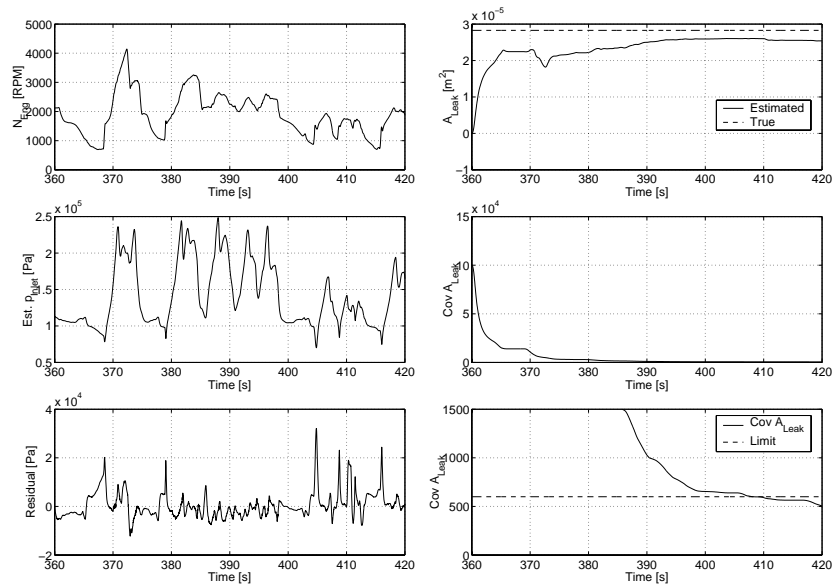


Figure 5.9: Manifold leakage filter with high inlet manifold pressure and 6 mm hole present.

5.3.1 Experimental results

The performance of the observers are in general better when the inlet manifold pressure is high, as was discussed in Section 5.2.5. During evaluation of the different observers, fix time intervals of 60 seconds have been used for estimation of the different parameters. For those cases with low excitation of the system, this time was not long enough to give good estimations.

One idea which have been examined in this master thesis project, is to use the covariance function of the estimated fault-parameter and from this draw an conclusion if the estimation is good enough and therefore stop the estimation.

One example. In Figure 5.9 are the engine speed, estimated inlet manifold pressure, the residual, estimated leakage area \hat{A}_{Leak} , solid line, together with the true leakage area, dashed line, and the covariance of \hat{A}_{Leak} been plotted. In this case there is a 6 mm hole present in the inlet manifold. The estimated leakage area is approximately $2.55 \cdot 10^{-5} m^2$ which indicates a hole diameter of 5.7 mm, close to the true size of the hole. When studying the covariance of \hat{A}_{Leak} in Figure 5.9 it is almost constant from 400 seconds an further on to the end, and the same is currently the case of the the estimated fault-parameter \hat{A}_{Leak} . In this case would a limit at 600 maybe be appropriate. When the covariance of the estimated parameter drops below this limit the estimation is said to be good and the simulation is aborted.

In Figure 5.10 we can see an additional case when the covariance of \hat{A}_{Leak} drops below the limit. In this case is it also the *ML*-filter with a 6 mm hole present in the inlet manifold but the inlet pressure is low during simulation. But when we study the value of \hat{A}_{Leak} the estimated leakage area is negative. The estimation is very bad, even though drops the covariance below the limit. Maybe the covariance is not a good way of deciding if the estimation is good.

5.3.2 Summary

In the first simulations shown in Figure 5.9 and 5.9 it seams that it could work but in Figure 5.10 we have an undesired behavior of the observer. Why does the covariance drop to such a low value even though the estimate is poor. It could be due to model errors. To study the covariance of the estimated parameter and from that come to a conclusion about if the estimated parameter is good, seams difficult. In this case the model errors are to large to be able to come to any conclusions. This will be even more difficult if there is another fault present that the observer was designed for. Further investigation of this is area is needed.

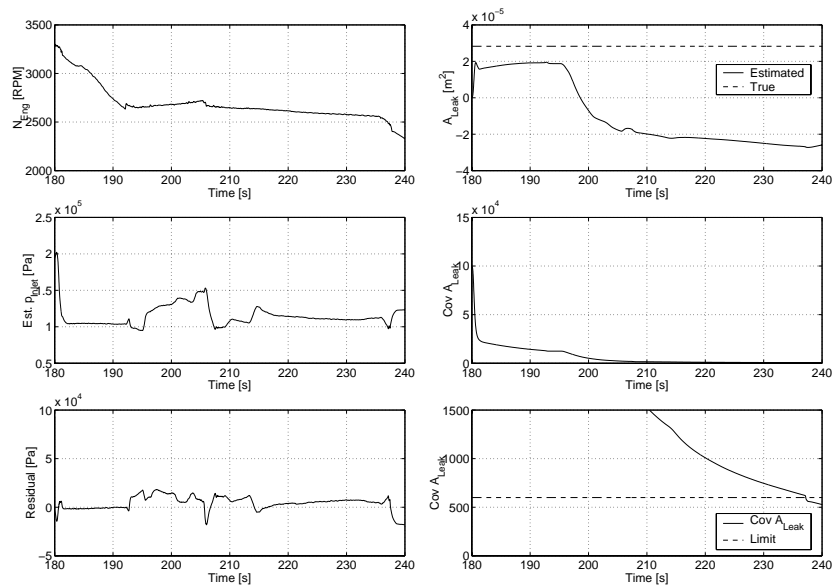


Figure 5.10: Manifold leakage filter with low inlet manifold pressure and 6 mm hole present.

Chapter 6

Conclusions and Future Work

6.1 Conclusion

Three different faults have been taken under consideration, air-mass flow sensor fault, inlet manifold pressure sensor fault and air-leakage in the inlet manifold. Inlet pressure sensor fault and mass-flow sensor fault are modeled as gain-faults. The mass-flow sensor fault is modeled in two different ways. Air leakage is modeled as a flow through a restriction.

The four different fault-models were linearized in *Mathematica* and the results were saved as *m*-files for *Matlab*. The extended Kalman filters were implemented in *Matlab/Simulink*.

The different filters have been evaluated with real data from a car driven on public roads. All filters, but especially the *HFM2* and *ML*-filters, have turned out to be sensitive to low mass-flows or low inlet manifold pressure. When the inlet pressure and the excitation of the system is low the result is effected in a negative way. On the other hand, during simulations with high inlet manifold pressure all filters produce good results. The estimated fault-parameters are close to the true value of the faults.

The idea of studying the covariance of the estimated fault-parameter to decide when to stop the simulation seems not to work. Even for bad estimations of the parameters the covariance drops to a low value and thus makes it hard to make the right decision.

The extended Kalman filter has turned out to perform well as an observer for a diagnosis system of an automotive engine. When the process-model corresponds well with the process, good estimations of the fault-parameters are produced.

6.2 Future Work

Some topics that can be looked upon at future work.

Further development of the engine model. The problems with estimating the fault-parameters during simulation with small variations in the inputs is probably due to model errors. Therefore would further development of the engine model be desirable.

Smoothers. Since the observer is working off-line, a nonlinear Kalman smoother could be interesting to investigate. A smoother is non-causal filter.

When should the simulation be stopped? The problem of when to stop the simulation by studying the covariance of the estimated parameter needs further investigation.

References

- [1] M. Nyberg, T. Stutte and V. Wilhelmi. Model based diagnosis of the air path of an automotive diesel engine. IFAC Workshop: Advances in Automotive Control, pages 255–260, Karlsruhe, Germany, 2001.
- [2] M. Nyberg and E. Frisk. Diagnosis and supervision of technical processes. Linköping, Sweden, 2001. Course material, Linköpings Universitet, Sweden.
- [3] Frank L. Lewis. *Optimal Estimation*. Wiley-Interscience publication. John Wiley & Sons, Inc, 1986.
- [4] Angus P. Andrews Mohinder S. Grewal. *Kalman Filtering: Theory and Practice*. Prentice-Hall Information and Systems Science Series. Prentice-Hall, Inc, 1993.
- [5] R. Klingmann., W. Fick, H. Brueggemann, D. Naber, K.H. Hoffmann, and A. Peters. Die neuen common-rail dieselmotoren mit direkteinspritzung in der modellgepflegten e-klasse. *Motortechnische Zeitung, MTZ*, (7,8,9), 1999.
- [6] John B. Heywood. *Internal Combustion Engine Fundamentals*. McGraw-Hill series in mechanical engineering. McGraw-Hill, 1992.
- [7] L. Guzzella and A. Amstutz. Control of diesel engines. *IEEE Control Systems*, pages 53–71, October 1998.
- [8] M. Nyberg and A. Perkovic. Model based diagnosis of leaks in the air-intake system of an SI-engine. *SAE Paper 980514*, 1998.
- [9] A. Truscott, A. Noble, A. Cotta, and T. Stutte. Simulation of gas path faults in a VGT diesel engine for the development of diagnosis algorithms. SIA International Congress, pages 1026–1031, Lyon, France, 2000.

Abbreviations and Notation

Abbreviations

CAC	Charge Air Cooler
Cov	Covariance
EKF	Extended Kalman Filter
EGR	Exhaust Gas Recycling
OBD	On Board Diagnosis
RMS	Root Mean Square
RPM	Revolutions Per Minute
VGT	Variable Geometry Turbocharger
VNT	Variable Nozzle Turbine

Notation

Variable	Unit	Explanation
A_{EGR}	m^2	Effective area of EGR valve
A_{Leak}	m^2	Effective leakage area
$c_{p,Air}$	$J/(kg \cdot K)$	Specific heat at const. pres. of air
$c_{p,Exh}$	$J/(kg \cdot K)$	Specific heat at const. pres. of exhaust gas
$c_{p,Inlet}$	$J/(kg \cdot K)$	Specific heat at const. pres. of gas in intake manifold
$c_{v,Air}$	$J/(kg \cdot K)$	Specific heat at const. vol. of air
$c_{v,Exh}$	$J/(kg \cdot K)$	Specific heat at const. vol. of exhaust gas
$c_{v,Inlet}$	$J/(kg \cdot K)$	Specific heat at const. vol. of gas in intake manifold
m_{Air}	kg	Mass of air in intake manifold
m_{EGR}	kg	Mass of EGR-gas in intake manifold
m_{Exh}	kg	Mass of exhaust gas in exhaust manifold
N_{Eng}	min^{-1}	Engine speed
R_{Air}	$J/(kg \cdot K)$	Gas constant of air
R_{Exh}	$J/(kg \cdot K)$	Gas constant of exhaust gas
R_{Inlet}	$J/(kg \cdot K)$	Gas constant of gas in intake manifold
p_{Atm}	Pa	Atmospheric pressure
p_{Exh}	Pa	Pressure in exhaust manifold
p_{Inlet}	Pa	Pressure in intake manifold
Q_{LHV}	J/kg	Lower Heating Value
T_{EGR}	K	Temperature of EGR gas-flow into the intake manifold
T_{Exh}	K	Temperature in exhaust manifold
T_{Inlet}	K	Temperature in the intake manifold
T_{Inter}	K	Temperature of the air after the charge-air cooler
V_{Eng}	m^3	Engine displacement
V_{Exh}	m^3	Volume of exhaust manifold
V_{Inlet}	m^3	Volume of intake manifold
W_{EGR}	kg/s	EGR mass-flow into intake manifold
W_{Exh}	kg/s	Exhaust mass-flow into the exhaust manifold
W_{Fuel}	kg/s	Mass-flow of injected fuel
$W_{Fuelmap}$	kg/s	Nominated mass-flow of injected fuel
W_{HFM}	kg/s	Air mass-flow past the air mass-flow sensor
W_{Inlet}	kg/s	Mass-flow into engine inlet-ports
W_{Leak}	kg/s	Mass-flow thru a hole
W_{Turb}	kg/s	Exhaust mass-flow past the turbine
X_{VNT}	%	Position of VNT vanes
κ	c_p/c_v	Ratio of specific heats